

Electronic Supplementary Information (ESI) for

**Bandgap engineering through nanocrystalline magnetic alloy grafting on
graphene[†]**

D. De,^{a,b} M. Chakraborty,^a S. Majumdar^a and S. Giri^{*a}

^a Department of Solid State Physics, Indian Association for the Cultivation of Science, Jadavpur, Kolkata 700 032, INDIA

^b Department of Physics, NITMAS, Diamond Harbour Road, 24 PGS (s), W.B., India

*Corresponding author's E-mail: sspsg2@iacs.res.in

I. SYNTHESIS PROCEDURE

Sequential stages of synthesis of grafting of Co₈₀Ni₂₀ on single layer of RGO is displayed in Figure S1.

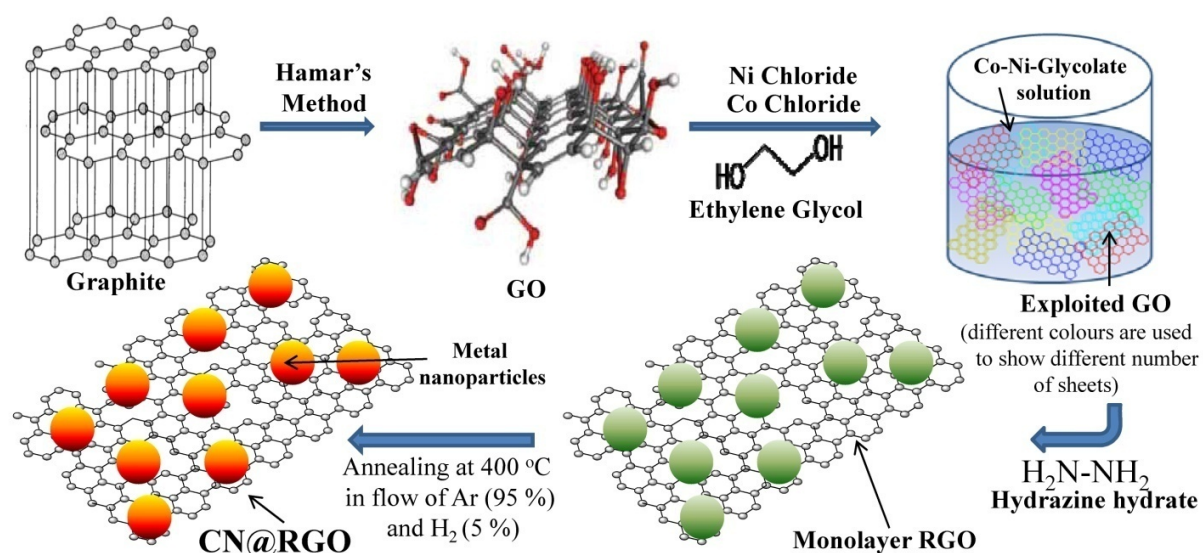


Figure S1: Sequential stages of synthesis of grafting of Co₈₀Ni₂₀ on single layer of RGO.

II. THERMOGRAVIMETRIC ANALYSIS (TGA)

Thermogravimetric analysis (TGA) is done in TA Instruments of SDT Q600 at a heating rate 10 $^{\circ}\text{C}/\text{min}$ in the N_2 atmosphere. Up to 400 $^{\circ}\text{C}$ CN1@RGO and CN5@RGO shows more stability than annealed RGO. Figure S2 shows that samples start to decompose above 400 $^{\circ}\text{C}$.

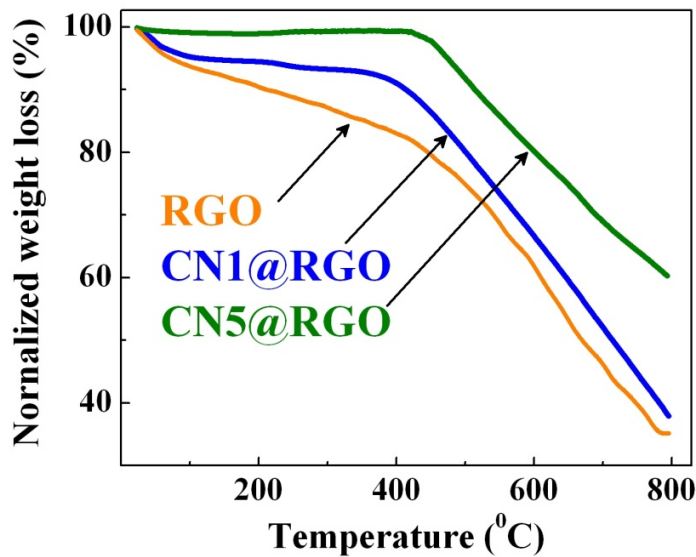


Figure S2: Variation of weight percentage with temperature of RGO, CN1@RGO and CN5@RGO.

III. FTIR SPECTROSCOPY

Fourier transform infrared spectroscopy (FTIR) is recorded in a Perkin-Elmer Spectrum 1000 IR Spectrometer at room temperature for annealed RGO, CN1@RGO and CN5@RGO, which are shown in Figure S3. The peaks corresponding to the stretching frequency of OH (3430 cm^{-1}) and bending frequencies corresponding to hydrated OH (1630 cm^{-1}) and alcoholic OH (1398 cm^{-1}) are evident for RGO. The epoxy peak appears at 1062 cm^{-1} for RGO. Analogous to the weak peak observed at 1630 and 1398 cm^{-1} , peaks appeared at 2920 and 2975 cm^{-1} correspond to the stretching vibrations in RGO. The intensity of the epoxy peak at 1062 cm^{-1} for RGO decreases

systematically with increasing alloying. The peak at 1630 cm^{-1} disappears for CN5@RGO. A new peak appears for CN5@RGO at 1428 cm^{-1} . The region highlighted in Figure 2d is modified considerably, which is correlated with the alloying process.

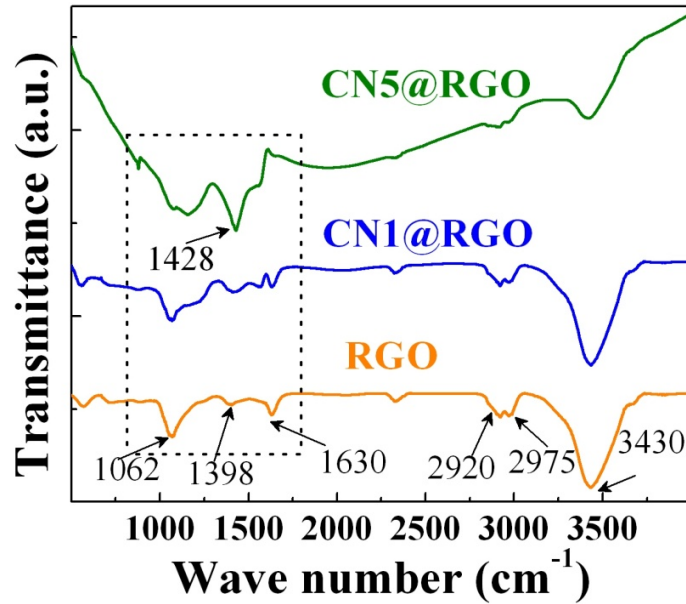


Figure S3: Fourier transform infrared (FTIR) spectroscopy for annealed RGO, CN1@RGO and CN5@RGO.

IV. X-RAY DIFFRACTION

Powder X-ray diffraction (XRD) studies are performed in a diffractometer, Seifert XRD 3000P with a Cu K α radiation source. Figure S4 shows XRD pattern of as synthesized and annealed RGO. We note that full width at half maximum (FWHM) corresponding to the peak (002) reduces remarkably due to annealing which signifies that annealing remarkably improves the crystalline state of RGO. Figure S4 (b) shows XRD pattern of as synthesized CN5@RGO where low intense peaks corresponding to Co₈₀Ni₂₀ nanocrystalline alloy coexist with RGO, which confirms concomitant reduction of RGO and Co-Ni alloy. Annealing improves the crystalline quality.

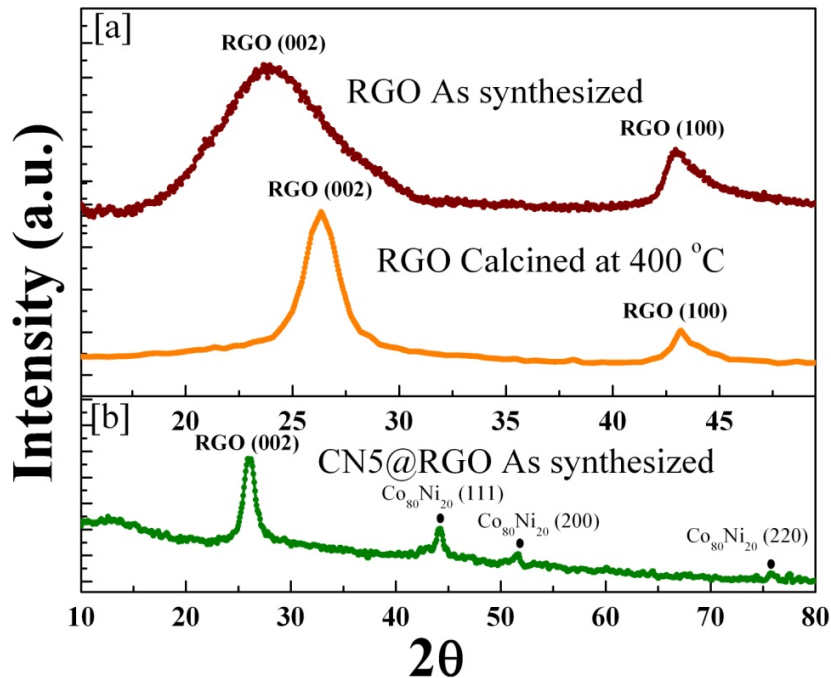


Figure S4: (a) XRD pattern of as synthesized and annealed RGO. (b) XRD pattern of as synthesized CN5@RGO.

V. TRANSMISSION ELECTRON MICROSCOPY (TEM)

Transmission Electron Microscopy (TEM) is performed using JEOL JEM, 2100F field emission microscope equipped with an energy dispersive x-ray spectrometer. Figure S5 shows various features of TEM images of annealed RGO, CN1@RGO and CN5@RGO. The TEM images in Fig.2 in the manuscript and Figure S5 in the SI show nearly homogeneous distribution in large area RGO sheets. From a good number of TEM images we can conclude that agglomeration was avoided and nearly separable distribution was achieved in all the samples with a distribution of particle size, which is shown in the histogram of the TEM image.

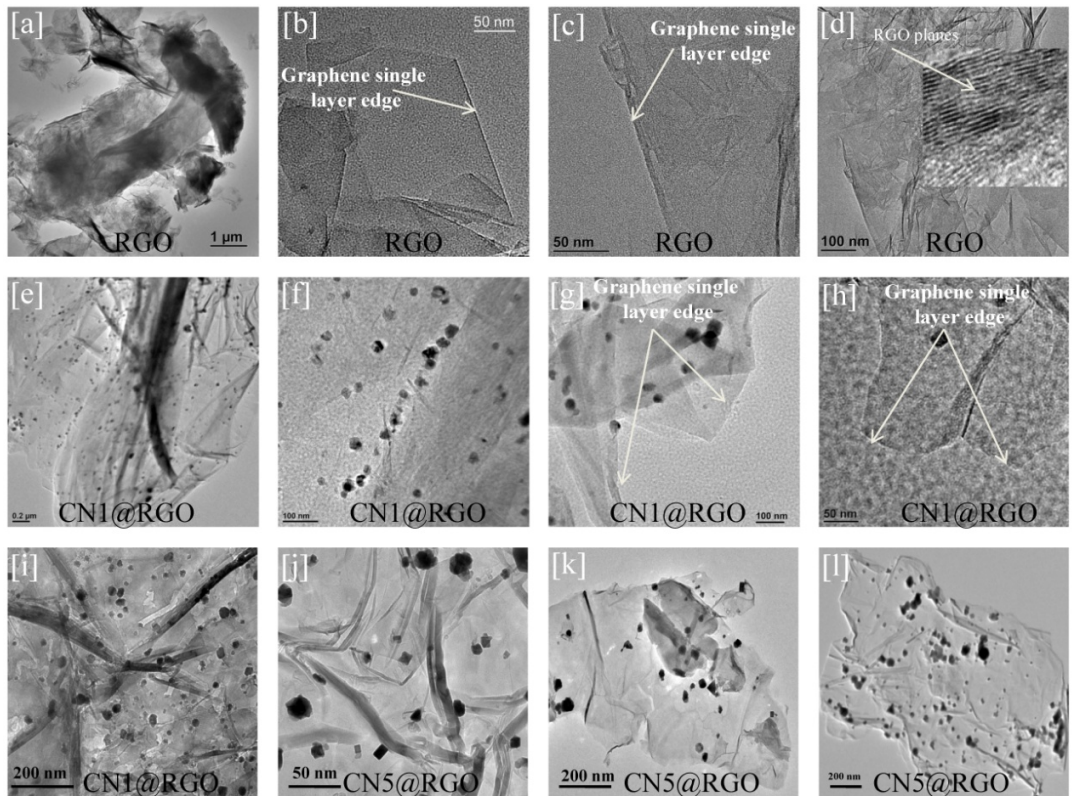


Figure S5: Various TEM images of annealed RGO, CN1@RGO and CN5@RGO.

VI. AFM STM Current-voltage characteristics

AFM STM Current-voltage characteristics is measured in VEECO DICP II autoprobe (model AP 0100). Figure S6 shows the $I-V$ curves recorded using STM technique. Powder samples of both CN1@RGO and CN5@RGO are dispersed in alcohol for several hours with sonication. Dispersed solution is deposited on HOPG substrate by drop casting. Systematic $I-V$ curves measured on different portions of the single layer graphene sheet and HOPG substrate are shown in Figure S6. Figure clearly shows that conductivity is decreased by ~ 10 times than the HOPG substrate.

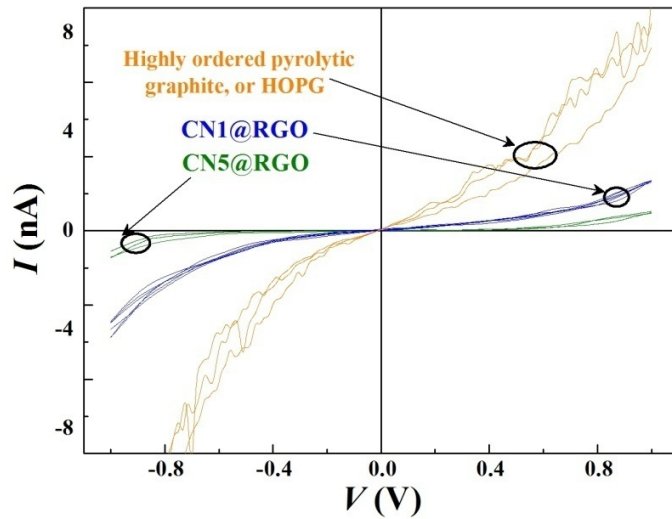


Figure S6: The I - V curves of CN1@RGO, CN5@RGO and HOPG.

VII. ULTRAVIOLET-VISIBLE (UV-VIS) SPECTROSCOPY

UV visible spectroscopy is measured in FRITSCH PULVERISETTE 7 premium line instrument. The ultraviolet-visible (UV-Vis) absorption spectroscopy is investigated to estimate optical bandgap. The absorption patterns of GO, annealed RGO, CN1@RGO and CN5@RGO are displayed in Figure S7. According to Tauc's formula, $(F_R h\nu)^{(1/n)} = K(h\nu - E'_g)$, bandgap energy (E'_g) can be obtained for a direct bandgap semiconductor, where $h\nu$ is the photon energy, $F_R = (1 - R^2)/2R$; R is the absorption coefficient and K is a constant. The linear plot of $(F_R h\nu)^2$ against photon energy typically provides E'_g . Intercepts of the extrapolation to x -axis directly provides E'_g . The values of this demonstrates that nanocrystalline alloy grafting tunes optical bandgap. Also similar plots are done from absorption spectroscopy. We plotted $(A/\lambda)^2$ or $\varepsilon^{(1/2)}/\lambda$ vs. photon energy (A and ε are the values of absorption corresponding to wavelength). In all the cases we got the increasing values of E_g with increase in alloying.

In the characterization of GO and RGO through UV absorption spectroscopy, both GO and RGO show strong optical absorption in the UV region, with a tail extending out into the

visible region, which is shown in Figure S7 of SI. In the UV-vis absorption spectrum of a GO, two different peaks appeared: a peak at 240 nm due to p-p* transition of aromatic C-C bonds and a shoulder at 300 nm assigned to n-p* transition of C-O bonds. In the case of graphene or RGO, the p-p* transition peak is red shifted to 280 nm and the n-p* transition peak disappeared. Due to the quantum confinement effect, the UV-vis spectra of GO or RGO reveal size dependent optical absorption. The value of the absorption intensity is given by the fine structure constant or its multiples as the number of graphene layers increases. However, our CN@RGO shows a systematic increase of optical bandgap with alloying. The monotonic increase in absorption in UV region, for GO, RGO and CN@RGO, is a result of light absorption by the multilayer graphitic domains. Appearance of optical bandgap in such a high conductive material is because of the edge effect. In two dimensional RGO sheet, with size of a few micrometers, the large surface to volume ratio is responsible for this. It is observed that, for RGO sheets of lesser sizes like Graphene Quantum Dots, the optical bandgap is much higher. Similarly, for CVD grown large area graphene sheets with moderate thickness, the optical bandgap reduces up to the order of 1 eV.

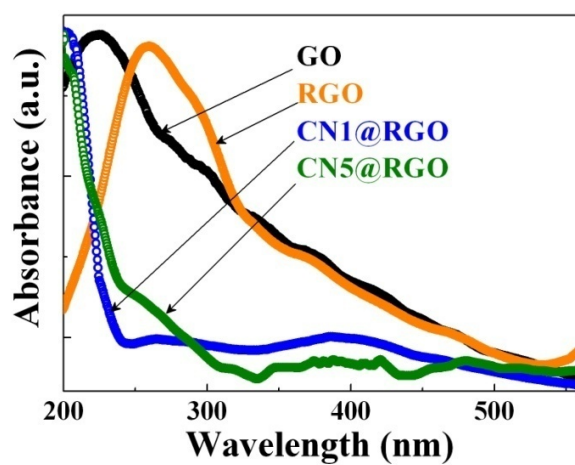


Figure S7: UV visible patterns of GO, RGO, CN1@RGO and CN5@RGO.

VIII. ELECTRICAL RESISTIVITY

Electrical resistivity (ρ) is measured using four probe technique on the pelletized samples of annealed RGO, CN1@RGO and CN5@RGO. Thermal variation of ρ exhibits typical manifestation of a semiconductor, although $\rho(T)$ could not be fitted in Arrhenius formalism [see Figure S8 of SI]. The values of ρ at 300 K are 7.7, 17.8 and 78.7 m Ω -cm for RGO, CN1@RGO and CN5@RGO respectively. This indicates that ρ increases systematically due to alloying. The disorder driven by alloying increases the localization of conductivity giving rise to the increase of ρ . According to Mott's variable-range hopping (VRH) model the polaron binding energy is small at low T ($T < \Theta_D/4$, Θ_D being Debye temperature)

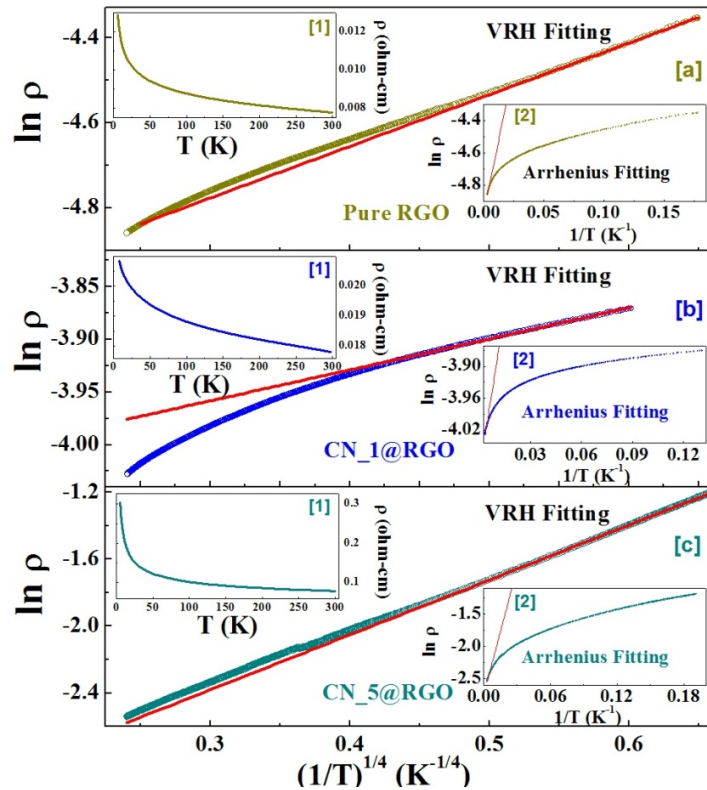


Figure S8: Plots of $\ln \rho$ with $T^{-1/4}$ for annealed RGO (top panel), CN1@RGO (middle panel) and CN5@RGO (bottom panel). All inset [1] depicts the plots of resistivity as a function of temperature. All inset [2] depicts the poor fitting with Arrhenius formalism.

and disorder energy plays a dominant role, where hopping may occur preferentially beyond nearest neighbors. The dc resistivity (ρ_{dc}) in the VRH model is defined as $\ln(\rho_{dc}/\rho_0) = (T_0/T)^{1/4}$, where ρ_0 and T_0 are constants. The fits using VRH formalism is demonstrated below 20, 35 and 40 K for RGO (top panel), CN1@RGO (middle panel) and CN5@RGO (bottom panel) respectively. This is in accordance with the satisfactory low- T fit using VRH formalism for disordered graphene nanoribbons. Temperature dependent activation energy (E_a) can be determined using, $E_a = (k/4)T_0^{1/4}T^{3/4}$, which provides $E_g=0.078$ and 0.79 meV for CN1@RGO and CN5@RGO respectively at 5 K. The results further demonstrate that alloying of RGO remarkably influences the E_g .